GeoHealth

RESEARCH ARTICLE

10.1029/2020GH000322

Key Points:

- Inter-annual variability of malaria in Mozambique is dominated by two spatio-temporal patterns
- These two spatio-temporal patterns are linked to the El Niño-Southern Oscillation and the Subtropical Indian Ocean Dipole
- Results suggest that predictable modes of inter-annual climate variability can be utilized to enhance malaria early warning systems

Supporting Information:

- Supporting Information S1

Correspondence to:

R. D. Harp,
ryan.harp@northwestern.edu

Citation:

Harp, R. D., Colborn, J. M., Candrinho, B., Colborn, K. L., Zhang, L., & Karnauskas, K. B. (2021). Interannual climate variability and malaria in Mozambique. *GeoHealth*, *5*, e2020GH000322. https://doi.org/10.1029/2020GH000322

Received 16 SEP 2020
Accepted 13 JAN 2021

Author Contributions:

Conceptualization: Ryan D. Harp, James M. Colborn, Kathryn L. Colborn, Lei Zhang, Kristopher B. Karnauskas
Data curation: Ryan D. Harp, James M. Colborn, Baltazar Candrinho, Kathryn L. Colborn, Kristopher B. Karnauskas
Formal analysis: Ryan D. Harp, Kristopher B. Karnauskas
Funding acquisition: Ryan D. Harp, Kristopher B. Karnauskas
Investigation: Ryan D. Harp, Kristopher B. Karnauskas
Methodology: Ryan D. Harp, James M. Colborn, Kathryn L. Colborn, Kristopher B. Karnauskas
Project Administration: Ryan D. Harp

Interannual Climate Variability and Malaria in Mozambique

Ryan D. Harp[1,2,3,4], James M. Colborn[5,6], Baltazar Candrinho[7], Kathryn L. Colborn[8,9], Lei Zhang[1], and Kristopher B. Karnauskas[1,2,10]

[1]Department of Atmospheric and Oceanic Sciences, University of Colorado Boulder, Boulder, CO, USA, [2]Cooperative Institute for Research in Environmental Sciences, University of Colorado Boulder, Boulder, CO, USA, [3]Institute for Sustainability and Energy at Northwestern, Northwestern University, Evanston, IL, USA, [4]Department of Earth and Planetary Sciences, Northwestern University, Evanston, IL, USA, [5]Clinton Health Access Initiative, Maputo, Mozambique, [6]The Climate Resiliency Group, Carbondale, CO, USA, [7]National Malaria Control Program, Maputo, Mozambique, [8]Department of Surgery, School of Medicine, University of Colorado Anschutz Medical Campus, Aurora, CO, USA, [9]Surgical Outcomes and Applied Research Program, University of Colorado Anschutz Medical Campus, Aurora, CO, USA, [10]Department of Environmental and Occupational Health, Colorado School of Public Health, Aurora, CO, USA

Abstract Malaria is among the greatest public health threats in Mozambique, with over 10 million cases reported annually since 2018. Although the relationship between seasonal trends in environmental parameters and malaria cases is well established, the role of climate in deviations from the annual cycle is less clear. To investigate this and the potential for leveraging inter-annual climate variability to predict malaria outbreaks, weekly district-level malaria incidence spanning 2010–2017 were processed for a cross-analysis with climate data. An empirical orthogonal function analysis of district-level malaria incidence revealed two dominant spatiotemporal modes that collectively account for 81% of the inter-annual variability of malaria: a mode dominated by variance over the southern half of Mozambique (64%), and another dominated by variance in the northern third of the country (17%). These modes of malaria variability are shown to be closely related to precipitation. Linear regression of global sea surface temperatures onto local precipitation indices over these variance maxima links the leading mode of inter-annual malarial variability to the El Niño-Southern Oscillation, such that La Niña leads to wetter conditions over southern Mozambique and, therefore, higher malaria prevalence. Similar analysis of spatiotemporal patterns of precipitation over a longer time period (1979–2019) indicate that the Subtropical Indian Ocean Dipole is both a strong predictor of regional precipitation and the climatic mechanism underlying the second mode of malarial variability. These results suggest that skillful malaria early warning systems may be developed that leverage quasi-predictable modes of inter-annual climate variability in the tropical oceans.

Plain Language Summary Malaria is one of the main public health concerns in Mozambique, with millions of reported cases in the country each year. While malaria has been tied to monthly swings in rainfall and temperature, its relationship to year-to-year changes of the climate is less well known. We identified regions where local malaria cases varied together and found two main patterns: a main hotspot over the southern half of Mozambique, and a second hotspot over the northern third of the country. Rainfall drives both of these hotspots. We then tied these patterns to two natural climate phenomena, the El Niño-Southern Oscillation and the Subtropical Indian Ocean Dipole, both of which impact the climate of the region and help drive malaria prevalence. Our results suggest that it may be possible to take advantage of the predictability of these climate phenomena to improve public health planning both in Mozambique and more broadly.

1. Introduction

The impact of climate and climate change on human health is increasingly recognized as one of the most pressing societal challenges. Many avenues for health-related climate impacts have been emphasized, including heat stress, extreme weather, air quality, freshwater availability, allergens, human conflict, vector-borne disease, and more (e.g., Watts et al., 2019). While many of the impacts of climate change on health

Resources: Ryan D. Harp, James M. Colborn, Baltazar Candrinho, Kathryn L. Colborn, Kristopher B. Karnauskas
Supervision: Kristopher B. Karnauskas
Validation: Ryan D. Harp, James M. Colborn, Kristopher B. Karnauskas
Writing – original draft: Ryan D. Harp, Kristopher B. Karnauskas
Writing – review & editing: Ryan D. Harp, Baltazar Candrinho, Kathryn L. Colborn, Lei Zhang, Kristopher B. Karnauskas

will be detrimental, these connections also present us with a public health opportunity. Increasing our understanding of the influences of interannual climate variability on infectious and vector-borne diseases can facilitate planning and resource allocation. One of the primary concerns among vector-borne diseases, and the focus of this study, is malaria.

1.1. Public Health Context

Malaria is the fourth leading cause of death among all infectious or parasitic diseases with ~450,000 deaths globally in 2016 (Centers for Disease Control and Prevention, 2018a; World Health Organization, 2018a). It is also directly linked to climate, primarily through precipitation (K. R. Smith et al., 2017b; Watts et al., 2019). As malaria is a vector-borne disease reliant on *Anopheles* mosquitoes for transmission, it is subject to the details of the *Anopheles* life cycle and is, thus, critically dependent on the existence of standing water. Adult *Anopheles* mosquitoes lay eggs in standing water which must neither dry out nor be flushed by excessive rainfall while larvae develop over a period of around 1–2 weeks (Centers for Disease Control and Prevention, 2018b). This results in malaria exhibiting a crucial dependence on the mean climate and its variability. The malaria transmission cycle is also influenced by temperature, which affects the speed at which both *Anopheles* mosquitoes and malaria parasites mature.

Malaria is endemic to Mozambique, a nation of over 30 million people on the southeastern coast of the African continent. There were 8.9 million reported cases of malaria in Mozambique in 2017, with annual reported deaths in the country due to malaria numbering in the low thousands (World Health Organization, 2018b). Consequently, Mozambique is one of six countries that collectively account for over half of all malaria cases globally (World Health Organization, 2020), as well as a focus country within the U.S. President's Malaria Initiative (Centers for Disease Control and Prevention, 2018c). In total, malaria led to 1.2 million disability adjusted life years lost in Mozambique in 2016, contributing 7% of all disability-adjusted life years lost that year in the country (World Health Organization, 2018a). These impacts are observed unevenly around the country due to spatial variability in both malaria incidence and population (Figure 1).

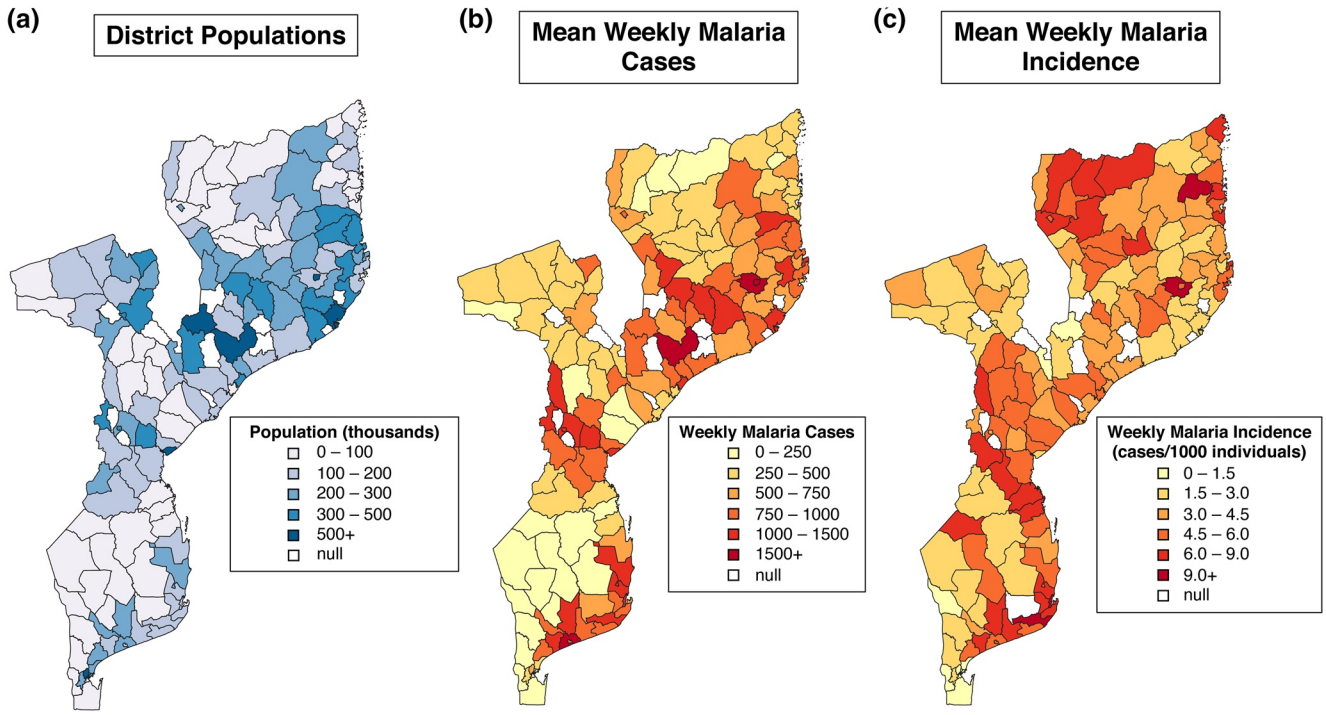

Figure 1. Distribution of Population and Malaria in Mozambique as of 2017. (a) Population for each district (blue fill). (b) Mean weekly cases of malaria for each district (yellow-red fill). (c) Same as (b) but for mean weekly incidence of malaria (cases per 1,000 individuals) for each district (yellow-red fill). Null values are due to recent redistricting within Mozambique.

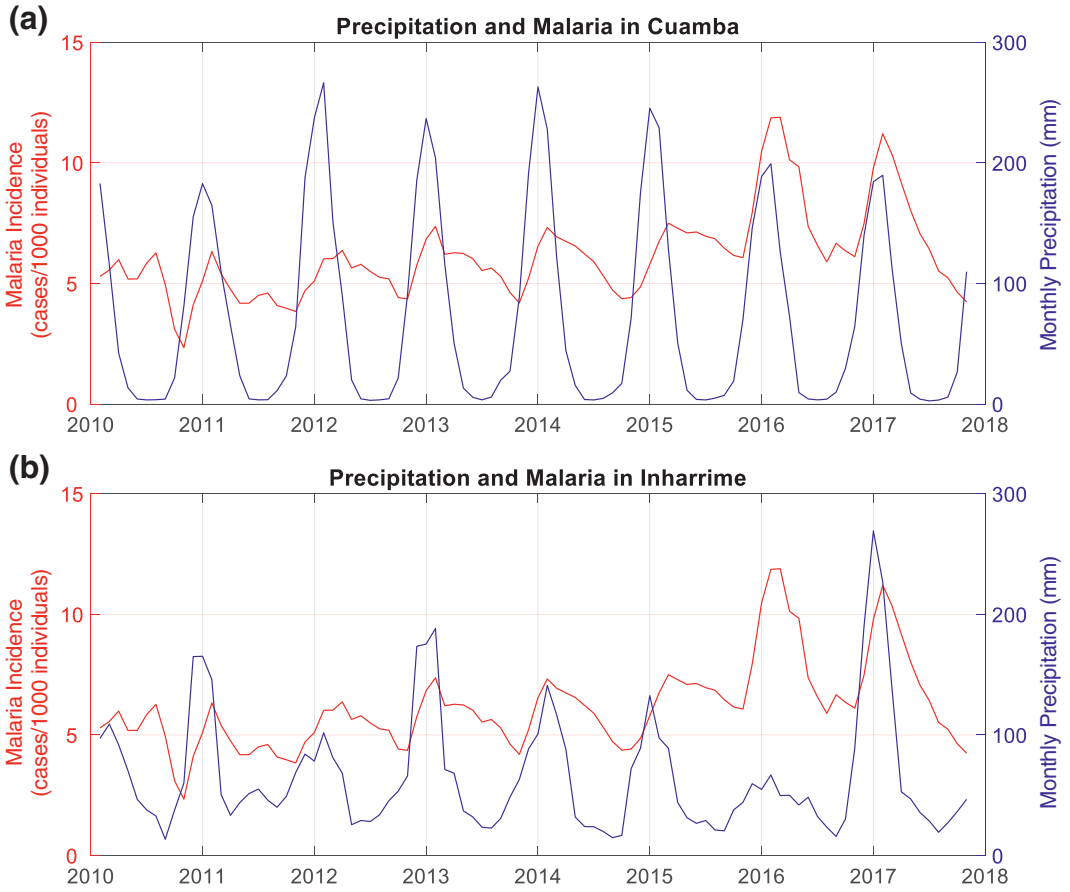

Figure 2. Malaria and precipitation in the Mozambique districts of Cuamba and Inharrime. (a) Three-month running means of malaria incidence (cases per 1,000 individuals) (red) and precipitation in mm/month (blue) for the district of Cuamba, Province of Niassa. (b) Same as (a) but for the district of Inharrime, Province of Inhambane.

Malaria transmission in Mozambique is highly seasonal with the peak in reported cases occurring several weeks after the onset of monsoonal rainfall during austral summer, as illustrated for two representative districts in Figure 2. Though the elapsed time between the onset of precipitation and the annual peak of the malaria outbreak varies with each district and year, a typical lag is roughly 6–10 weeks. Therefore, while seasonal precipitation in Mozambique peaks from November-April, the peak in malaria prevalence typically occurs around January-March.

There is potential human and economic value in increasing our understanding of how malaria incidence is affected by weather and climate (Thomson et al., 2018). For example, developing an effective and skillful malaria early warning system with sufficient lead time for public health applications could maximize preparedness and the efficient use of limited resources. Because of this, many efforts have aimed to develop a malaria early warning system that could inform public health responses for highly impacted countries (e.g., Girond et al., 2017; Merkord, 2017; Thomson et al., 2006; World Health Organization, 2001). While these attempts often utilize observed and forecasted weather and climate information, the usefulness of these inputs has yielded mixed results (Thomson et al., 2018). Conventional attempts to develop a malaria early warning system incorporating meteorological factors often aim to produce statistical models by focusing on short-term lead-times (i.e., weeks to 2 months of advance notice) between observed precipitation and temperature and their interactions with observed malaria incidence (e.g., Kim et al., 2019; Midekisa et al., 2012; Teklehaimanot et al., 2004; Xiang et al., 2018). Mabaso et al. (2012) critically reviewed 35 publications and noted that nearly all examined studies agreed that meteorological conditions were a crucial factor in malaria epidemics, with an overarching focus on precipitation. Of these, only six studies investigated potential linkages between the El Niño-Southern Oscillation (ENSO) and malaria epidemics in Africa, and those

studies yielded mixed results. However, recent efforts have increasingly shifted to examining the interactions between ENSO, along with other modes of interannual climate variability, and their influences on rates of malaria (e.g., Behera et al., 2018; Bouma & van der Kaay, 1996; Diouf et al., 2020; Ikeda et al., 2017; Kreppel et al., 2019; Landman et al., 2020; J. Smith et al., 2017a). In particular, the major tropical ocean basin on the eastern side of Africa, the Indian Ocean, holds considerable potential for predictability at the interannual time scale (e.g., Behera & Yamagata, 2001; Webster et al., 1999). This widening focus on establishing ties between interannual climate variability and malaria, with the potential for enhanced predictability and public health benefits, is the context for the present paper.

Mozambique is currently in the process of implementing a near-term early warning system to provide district-level predictions of malaria outbreaks. This system will utilize meteorological variables like temperature and precipitation, along with the spatiotemporal relationship between weekly aggregated district-level cases of malaria (Colborn et al., 2018), to provide predictions of outbreaks with a lead time of ~4 weeks. Although this lead time is expected to be sufficient to mobilize existing resources for outbreak mitigation and response within an affected area, it is not sufficient to alter long-term planning of operations such as indoor residual spraying or distribution of long-lasting insecticide-treated nets that are planned several months in advance in response to predicted transmission conditions. Given this, the government has expressed the need for a longer-term forecasting system that takes advantage of the potential predictability of interannual climate variability.

1.2. Meteorological and Climatic Context

Spanning 10°–27°S latitude, the country of Mozambique lies in both tropical and subtropical zones and thus possesses a transitional climate regime. The primary manifestation of the tropical-subtropical transition is a sharp north-south rainfall gradient, particularly in austral summer (Figure S1). The primary driver of precipitation in the northern part of the country is the annual penetration of the Intertropical Convergence Zone, reaching its southernmost extent around 15°S. The Intertropical Convergence Zone drives tropical precipitation rates (up to 800 mm per summer) for the northern part of Mozambique. South of the annual reaches of the Intertropical Convergence Zone, rainfall is less frequent and scarcer (200–300 mm per summer), and the climate is subtropical in characterization. In addition to mean state differences, there also exist discrepancies in the interannual variability in precipitation (Figure 2). To illustrate, the district of Cuamba lies in the northern part of the country (36.5°E, 14.7°S) and experiences more consistent precipitation during austral summer with minimal precipitation outside of the monsoon season. In contrast, Inharrime is in the southern part of the country (34.7°E, 24.4°S) and experiences both dramatic interannual variability in austral summer precipitation, as well as greater precipitation totals outside of the rainy season compared to Cuamba.

The ENSO is the dominant mode of climate variability in the tropics, with impacts felt around the globe (Rasmusson & Carpenter, 1983). The remote impacts of ENSO events begin as local changes to the atmospheric circulation and precipitation patterns over the equatorial Pacific Ocean, which then manifest in teleconnections around the globe, including into higher latitudes. Anomalously warm or cool sea surface temperatures (SSTs) over the eastern equatorial Pacific produce a cascading atmospheric response that propagates globally as both atmospheric Kelvin and Rossby waves (Gill, 1980; Hoskins & Karoly, 1981). Examinations of ENSO teleconnections indicate that El Niño (La Niña) is likely to reduce (increase) precipitation over southern Africa due to shifting atmospheric circulation patterns over the region (Cane et al., 1994; Hoell & Cheng, 2018).

In addition to ENSO, there are a number of modes of climate variability that impact southern Africa. One of these modes of climate variability is the Indian Ocean Dipole (IOD), an oscillation of warmer and cooler SSTs over the equatorial Indian Ocean (Saji et al., 1999; Webster et al., 1999). The positive (negative) phase of the IOD has anomalously warm (cool) SSTs and increased (decreased) precipitation over the western Indian Ocean and surrounding region. While perhaps not as dominant of a driver of global climate anomalies as ENSO, the IOD does have strong influences on the climate over the surrounding region, including western Africa, India, Southeast Asia, and Australia (e.g., Ashok et al., 2001, 2003; Saji & Yamagata, 2003). Distinct from the IOD is the Subtropical Indian Ocean Dipole (SIOD). First identified by Behera and Yamagata (2001), the SIOD consists of a pattern of oscillating SSTs between poles southeast of Madagascar and

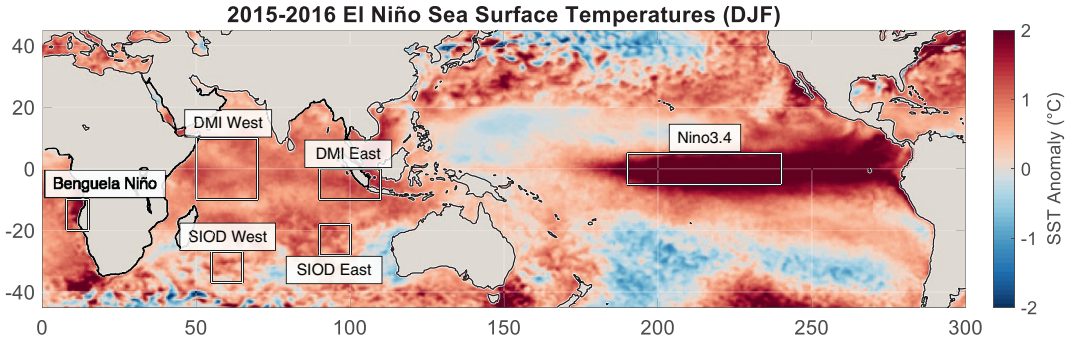

Figure 3. Climate Index Definitions. Map of December, January, and February SST anomalies during the 2015–2016 El Niño event (blue-red fill). Boxes illustrate domains of spatial averaging involved in calculating indices for the various modes of climate variability described in the main text and Table S1. SST, sea surface temperatures.

west of Australia (Figure 3). This oscillation induces regional impacts on precipitation, namely to southern Africa, where a positive SIOD—that is, warm SST anomalies to the southwest of Madagascar—leads to increased precipitation over southern Africa (Hoell et al., 2018; Reason, 2001). Benguela Niños occur when anomalously warm waters persist off the western coasts of Namibia and Angola, near the confluence area of the Angola Current and the Benguela upwelling system (Florenchie et al., 2003; Reason et al., 2006; Shannon et al., 1986). Further afield, Benguela Niños also can lead to altered precipitation patterns across southern Africa (Hansingo & Reason, 2009; Reason & Smart, 2015; Rouault et al., 2003). Finally, the Southern Annular Mode, also known as the Antarctic Oscillation, describes the zonal position of a band of westerly winds encircling the Antarctic continent (Gong & Wang, 1999; Marshall, 2003), and can similarly influence precipitation in southern Africa, among other locations (Gillett et al., 2006; Hendon et al., 2007). Though not examined here, there is some evidence of a multidecadal pattern in southern African rainfall as well (Morioka et al., 2015; Reason & Rouault, 2005). The modes of climate variability mentioned above represent likely candidates to bridge climate and malaria in Mozambique, but it should be noted that our methodology does not assume *a priori* that one or more modes are responsible for this linkage; they are confirmed independently and objectively through an analysis process that begins with malaria itself.

2. Data and Methodology

2.1. Malaria Data

Weekly counts of laboratory-confirmed malaria cases at health facilities from 2010 to 2017, reported through the Boletín Epidemiológico Semanal, were secured through the National Malaria Control Program of Mozambique. The high temporal resolution data set is reported in epidemiological weeks, a standardized method of grouping data by continuously counted weeks. Aggregated health facility data are reported for each of 148 individual administrative districts in Mozambique, producing a relatively fine-scale spatial resolution compared to most global climate observations.

Epidemiological week level data provided for each district includes the date, district and province codes, total confirmed cases of malaria, confirmed cases of malaria for those under and over 5 years of age, and total district population. Analysis for endemic diseases often focuses on cases for children under 5 years of age (e.g., Colborn et al., 2018) as it can provide a better representation of disease prevalence than total cases since many previously infected adults do not need or seek treatment for subsequent infections later in life. In addition, children under 5 years of age are among the most vulnerable subpopulations, accounting for around two-thirds of all deaths from malaria (World Health Organization, 2020). Since our methodology required the use of malaria incidence (cases per population within each district), and age demographics for specific districts were incomplete (i.e., number of individuals under age 5), it was necessary to utilize the total number of cases across all age groups. However, a comparison of total cases versus cases in children under five revealed a correlation of 0.93 and it is unlikely that this necessary modification altered any results or conclusions.

2.2. Climate Data

Time-varying climate fields were derived from a number of sources. Precipitation data were gathered from both the Climate Hazards Group Infrared Precipitation with Station (CHIRPS; Funk et al., 2014) and NOAA's Global Precipitation Climatology Project (GPCP; Adler et al., 2003). The CHIRPS data set is designed to provide relatively high spatial resolution (0.05° or ~5 km) precipitation observations with near-global spatial coverage (50°N-50°S) at several temporal scales from 1981 to present. Originally developed to support work for the Famine Early Warning Systems Network, CHIRPS combines remote sensing rainfall estimates from the Tropical Rainfall Measuring Mission with multiple sources of station gauge data to create a gridded precipitation time series (Funk et al., 2015). We coarsened daily CHIRPS data both spatially and temporally to produce a 0.5° (~50 km) monthly data set over the domain of interest. Precipitation data were also taken from the fully global GPCP version 2.3 data set. Similar to the construction of the CHIRPS data set, the GPCP data set blends precipitation estimates from remotely sensed microwave and infrared data with surface rain gauge observations to produce a monthly data set at 2.5° (~250 km) resolution from 1979 to present (Adler et al., 2003). In addition to providing global spatial coverage, GPCP data also provide a validation check for the CHIRPS observation data. SST data were pulled from the NOAA Optimum Interpolated version 2 (OIv2) product. OIv2 is a relatively high resolution (0.25°) daily product created by blending buoy and ship observations with two sources of satellite SST data (Reynolds et al., 2002, 2007).

For a more comprehensive description of global and regional climate variability, we also used output from a state-of-the-art gridded reanalysis product—the European Centre for Medium-Range Weather Forecasts (ECMWF) Reanalysis 5 (ERA5). Reanalyses incorporate historical meteorological observations from an array of sources, including data from geostationary satellites, surface measurements, buoys, radiosondes, and aircraft data (see Tables 14–16 of ERA5 documentation for full list of assimilated data sources; Hennermann & Berrisford, 2017). These observations are used to confine a time-evolving global weather model to produce a gridded data set of a wide variety of meteorological variables with the aim of overcoming conventional issues with the spatial distribution of observations and shortcomings of unconstrained models (Dee et al., 2011). ERA5 is the latest reanalysis produced by ECMWF and is the successor to the widely used ERA-Interim reanalysis product (Hersbach et al., 2019). Climate variables used from ERA5 span the globe from 1979 to present at a spatial resolution of 0.25°; our analysis extends through 2019. The atmospheric variables from ERA5 included in our analysis are 300 hPa geopotential height; 500 hPa geopotential height, vertical velocity; 700 hPa geopotential height; 850 hPa geopotential height, specific humidity, wind vectors; 10 m wind vectors; 2 m temperature, dew point; surface mean sea level pressure, precipitation; and vertically integrated moisture flux divergence (Copernicus Climate Change Service, 2017).

2.3. Data Processing and Methodology

Malaria incidence in Mozambique exhibits a distinct seasonal cycle (Figure 2). Unlike the relatively smooth annual cycle exhibited by many climate variables (e.g., temperature), the asymmetric seasonal cycle (i.e., abrupt onset of high-malaria season and more gradual decline) of malaria within districts is problematic for the application of conventional climate data analysis techniques. For example, the initial onset of malaria can vary dramatically across years, rendering a simple, average climatological cycle ill-suited and something as simple as a slightly later-than-average onset may appear as a pronounced anomaly. In addition, the district-level baseline of malaria varies annually, though it typically stays above zero cases given its endemicity in Mozambique.

For a robust description of the spatiotemporal variability of malaria within Mozambique, we applied an empirical orthogonal function (EOF) analysis (a.k.a. Principal Component Analysis) to the full complement of Mozambique malaria data. Before implementing the EOF analysis, we employed several quality control and data preprocessing steps. First, we accounted for missing data by (1) removing six recently created districts from our analysis that possessed an insufficient length of reported data, and (2) linearly interpolating over 42 missing data points. The second step, which was necessary to execute the EOF analysis, accounted for less than a tenth of a percent of the remaining data. After accounting for missing data, we divided the total malaria case number in a given week by the population of each district. This allowed us to overcome analysis difficulties caused by the high variability of district case numbers that may merely reflect the higher population of the district. For illustration, note the differences evident in Figure 1 between mean weekly

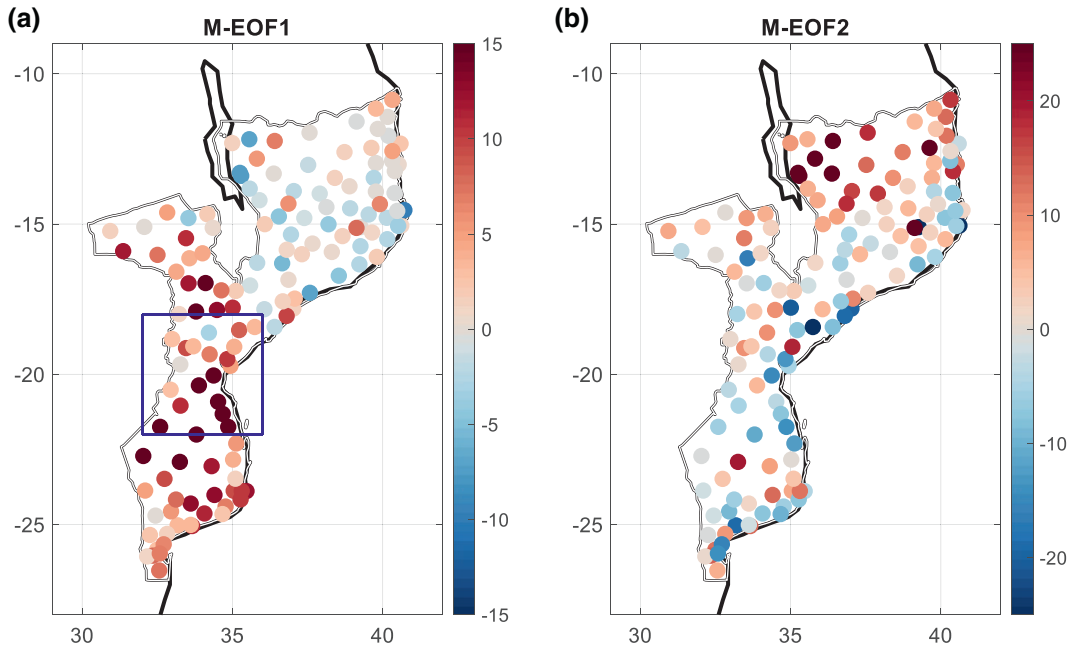

Figure 4. Dominant modes of spatio-temporal variability in interannual malaria incidence. (a) Primary mode of spatiotemporal variability (M-EOF1) where each dot represents the loading for a district. This mode explains 63.5% of the spatiotemporal variance of interannual malaria incidence. Borders of precipitation index are outlined in blue. (b) Same as (a) but for M-EOF2. This mode explains 17.1% of the spatiotemporal variance of interannual malaria incidence. EOF, empirical orthogonal function.

cases of malaria and mean weekly incidence of malaria. To isolate the interannual variability in malaria rates and account for the inconsistent seasonality of the malaria time series, we then applied an annual (53-week period) low-pass filter to data for each district. Finally, we removed the mean and detrended the malaria incidence time series by removing a third-order polynomial. This final step accounts for variability occurring at time scales beyond interannual variability, such as known changes in testing frequency. An EOF analysis was then applied to these clean, quality-controlled, district-level time series of malaria. A second EOF analysis of precipitation was also performed on the coarsened CHIRPS data set, though the amount of preprocessing required was less extensive. In addition to applying a 53-week low-pass filter, the precipitation data was also subset spatially and temporally for austral summer in Mozambique. Limiting the analysis of precipitation to austral summer facilitates specific examination of the time period of precipitation driving the annual cycle of malaria.

There are a number of ways to describe the implementation and results of an EOF analysis or PCA depending in part on the academic field. We note for clarity that we will be adopting the terminology described by Björnsson and Venegas (1997). Accordingly, the spatial patterns of variance will be referred to as EOFs and their corresponding time series of weighting will be referred to as PCs (principal components). The EOF (PC) which explains the most and variance will be referred to as EOF1 (PC1), etc. Finally, we append an M- or P- prefix to specify discussion of the results of malaria or precipitation EOF analyses, respectively.

3. Results

3.1. Primary Spatio-temporal Patterns of Malaria and Precipitation in Mozambique

The two leading EOF modes of malaria incidence (M-EOF1, M-EOF2) explain 64% and 17% of the interannual variability, respectively. M-EOF1 reveals a roughly north-south split at ~17°S with a prominent center of action in the southern part of Mozambique and a weaker center of action in the north (Figure 4). M-EOF2 describes a pattern with an action center north of 15°N and a weak center of action or neutral response in the south. It should be noted that the region of these cut-offs (17°S and 15°S, respectively) roughly correspond to the southerly extent of the Intertropical Convergence Zone complex. Collectively,

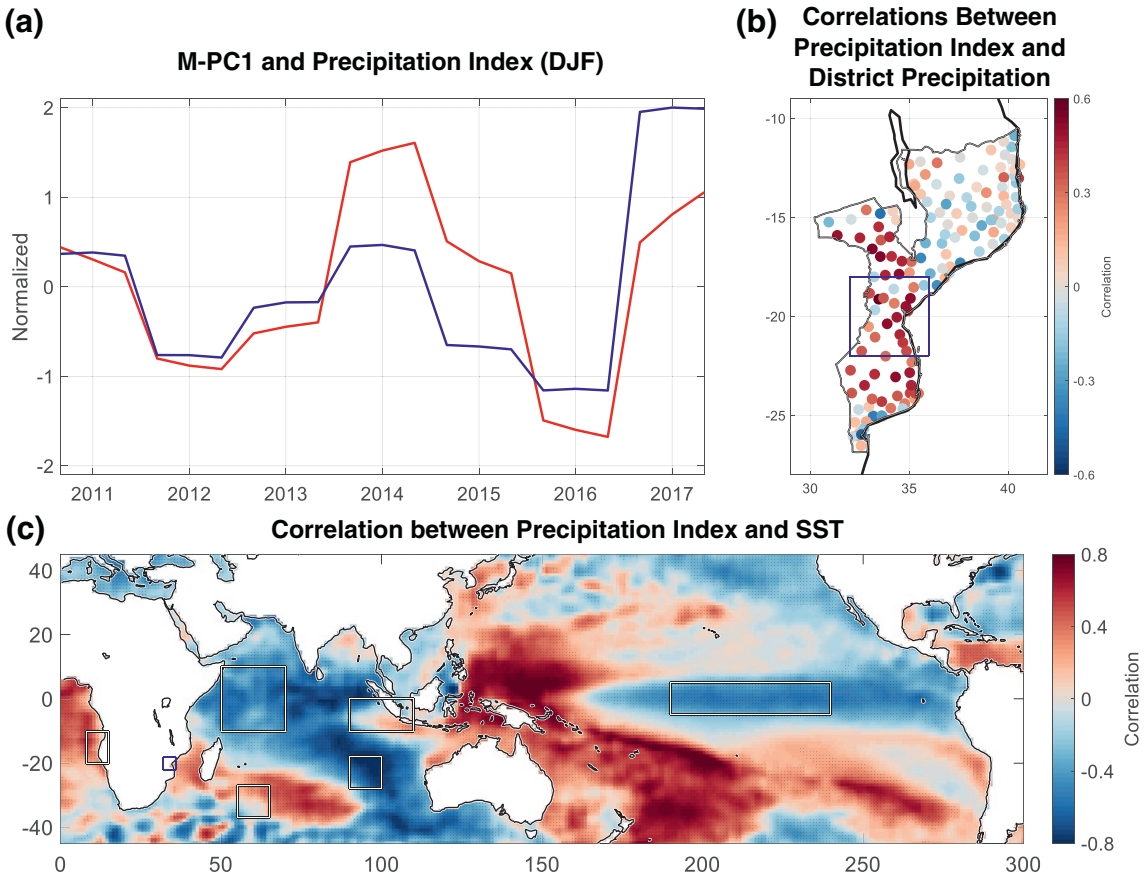

Figure 5. Analysis of a Central Mozambique Precipitation Index. (a) Normalized values of M-PC1 (red) and precipitation index (blue). Monthly values are shown for all austral summer months from December 2010 to February 2017 ($p < 0.001$). (b) Correlation between precipitation index (mean precipitation within blue outline) and district precipitation (blue-red filled circles). Note similarities to the spatiotemporal pattern of M-EOF1 in Figure 4a. (c) Correlations between mean monthly precipitation within central Mozambique precipitation index box (blue box, same as in b) and SSTs (blue-red fill) from 2010 to 2017 after application of a 13-month low-pass filter. Stippling denotes regions where significance exceeds $p < 0.05$. Boxes illustrate locations of spatial averaging involved in calculating indices for various modes of climate variability (ENSO, IOD, SIOD, and Benguela Niño) as defined in Table S1. ENSO, El Niño-Southern Oscillation; IOD, Indian Ocean Dipole; SIOD, Subtropical Indian Ocean Dipole.

the spatiotemporal patterns revealed by the EOF analysis show that the leading mode of interannual variability in malaria incidence in Mozambique is a concentrated fluctuation between high and low rates in the southern half, with weaker, out-of-phase, variability in the north. The results of the same EOF analysis with malaria incidence for individuals under age five produced nearly identical patterns (Figure S2).

Both principal components were compared against indices describing the state of the aforementioned modes of climate variability: El Niño-Southern Oscillation, IOD, SIOD, Benguela Niño, and the Southern Annular Mode. These climate indices were calculated directly from global SST observations using standard definitions (Figure 3 and Table S1). While M-PC1 did not demonstrate obvious statistical relationships with any of the climate indices over the relatively limited time span of the malaria observations, M-PC2 was strongly anticorrelated with the IOD ($r = -0.80$), though we demonstrate this relationship to be spurious in Section 3.3.

To further investigate how the M-EOF1 *physically* relates to global, interannual climate variability, a new precipitation index was constructed by averaging rainfall over central Mozambique (from 32°E–36°E to 18°S–22°S; see Figure 4a). The resulting projection of the precipitation field onto the precipitation index is highly correlated with both the spatial loading pattern of M-EOF1 and M-PC1(Figures 5a and 5b). Establishing a precipitation index as a proxy for M-EOF1 allows for an investigation of conditions that lead to M-EOF1, but over a greater time span; while available malaria data only spans from 2010 to 2017, multiple high-quality precipitation data sets span from ~1980 to present. This lengthened time span facilitates a

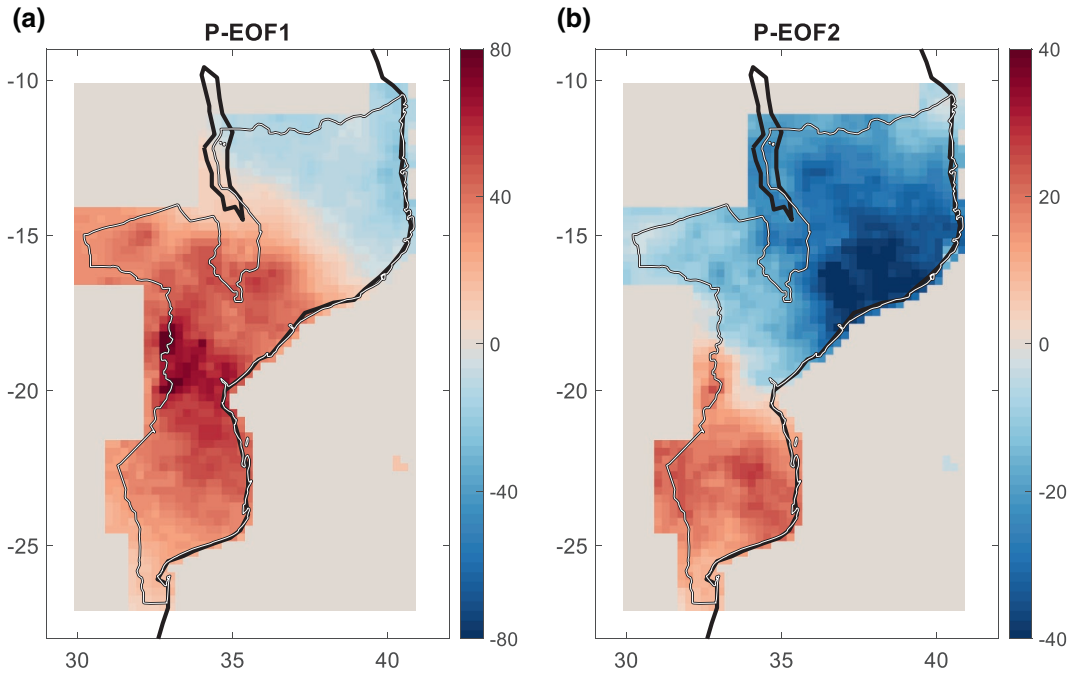

Figure 6. Dominant modes of spatiotemporal variability of austral summer precipitation in Mozambique. (a) Primary mode of spatiotemporal variability (P-EOF1) of mean austral summer precipitation from 1982 to 2018. This mode explains 45.6% of the spatiotemporal variance. (b) Same as (a) but for P-EOF2. This mode explains 17.1% of the spatiotemporal variance. Note also the spatial correspondence with malaria EOFs (Figure 4). EOF, empirical orthogonal function.

more robust exploration of relationships between Mozambique malaria/precipitation and modes of climate variability. Given that climate phenomena such as the ENSO and the IOD oscillate with return periods between 1 and 10 years, a roughly 40-year analysis period allows for a more robust analysis than is afforded by the comparatively short 8-year time period, the latter of which encompasses a limited number of cycles of the modes of climate variability under investigation and may be confounded by nonstationarity.

To determine which mode of climate variability underlies the variability represented by the central Mozambique precipitation index, we calculated and mapped the correlation between the precipitation index and global SST (Figure 5c). This analysis reveals a statistically significant SST anomaly pattern closely projecting onto the canonical fingerprint of La Niña. A high precipitation index value corresponds to a warmer (cooler) than average western (eastern) equatorial Pacific Ocean; the central Mozambique precipitation and Niño 3.4 climate indices are highly correlated ($r = -0.57$, $p < 0.001$). This analysis also reveals potential links between central Mozambique precipitation and the SIOD, the IOD, and the Benguela Niño, which are further examined through the EOF analysis of precipitation.

The primary mode of austral summer precipitation (P-EOF1) mirrors M-EOF1, with a loading maximum centered over the region of the precipitation index (Figure 6). P-PC1 is significantly correlated with the Niño 3.4 index ($r = -0.63$, $p < 0.001$). Taken together, these EOF analyses on malaria and regional precipitation suggest a link between ENSO and malaria/precipitation where La Niña (El Niño) events typically lead to increased (decreased) precipitation over the southern, subtropical portion of Mozambique. Additional modes of interannual climate variability in the Indian Ocean (e.g., the SIOD) are also implicated and require further examination. The physical mechanisms underlying the linkages suggested by these temporal correlations are examined further in the following section.

3.2. Diagnosis of the ENSO Influence on Mozambique Rainfall and Malaria

The connection of El Niño (La Niña) to a drier (wetter) austral summer over southeastern Africa is a known teleconnection (e.g., Cane et al., 1994; Ropelewski & Halpert, 1987). However, to fill a gap within the

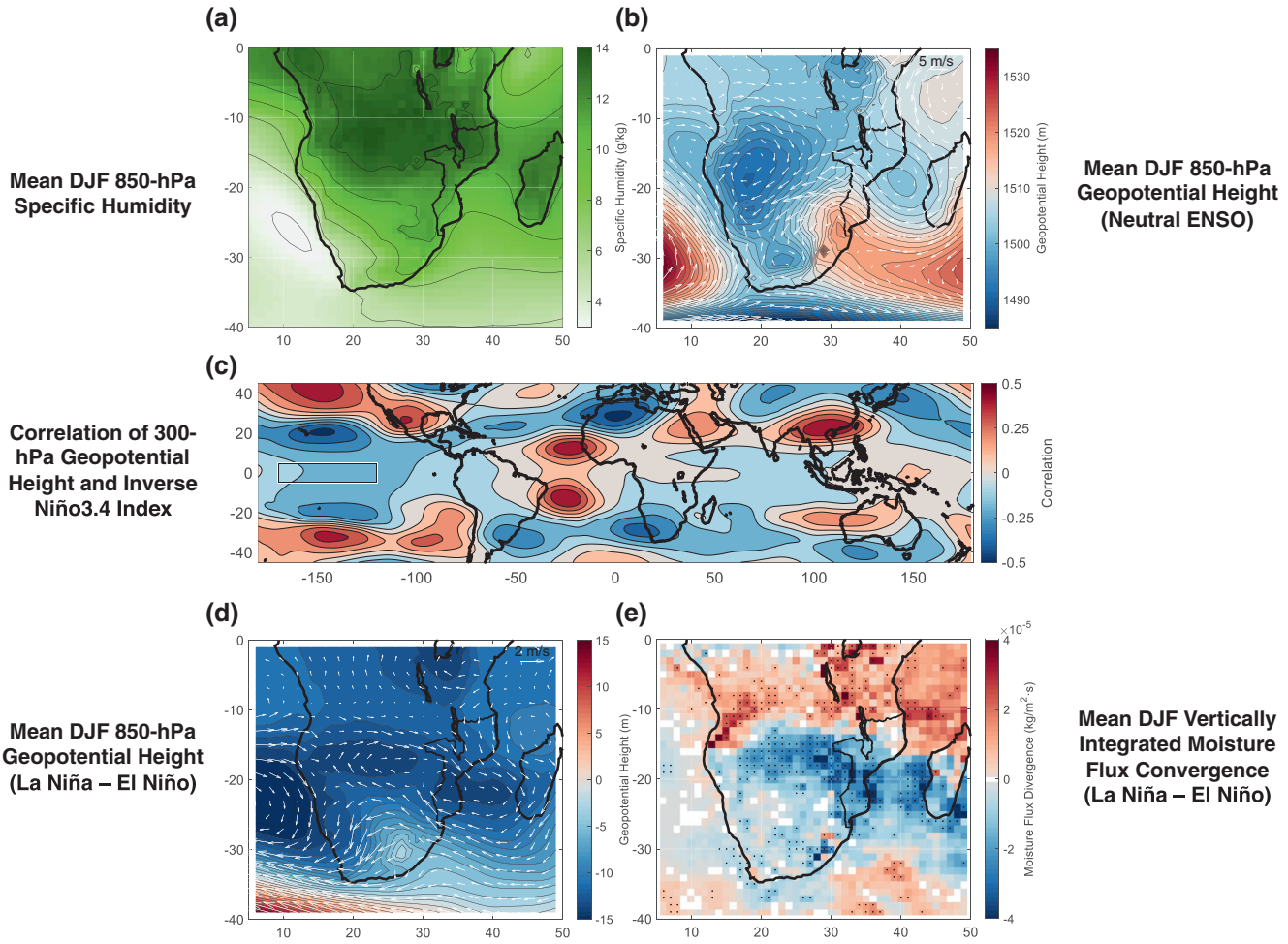

Figure 7. Climate diagnosis of ENSO influence on Southern Africa during austral summer. (a) Mean austral summer specific humidity at 850 hPa in g/kg (green fill). Contours every 2 g/kg beginning at 3 g/kg. (b) 850 hPa geopotential height and winds in austral summer during neutral ENSO conditions. Geopotential height in m (red-blue fill) with contours every 1.65 m. Wind vectors (white arrows) in m/s. (c) Correlations between austral summer Niño 3.4 Index and 300 hPa geopotential height minus zonal mean (red-blue fill). Contours every 0.1. Niño 3.4 Index box plotted over the equatorial Pacific (black). (d) Same as (b) but for a composite of La Niña-El Niño events. 31 evenly spaced contour intervals. Wind vectors (white arrows) in m/s. (e) Mean austral summer vertically integrated moisture flux divergence for composite of La Niña-El Niño events. Moisture flux divergence (blue-red fill) is in kg/m^2 s with 13 evenly spaced contour intervals. Stippled values exceed two-sigma significance. ENSO, El Niño-Southern Oscillation.

literature surrounding the link between ENSO and precipitation—and subsequently, malaria—over subtropical Mozambique, it is necessary to establish the mechanistic links between ENSO and its downstream influence on southern Africa. We explain and illustrate our dynamical diagnosis of this mechanism here.

One major source of moisture for subtropical Mozambique in austral summer is the tropical southern Congo Basin (Figure 7a). Much of the austral summer rainfall in Mozambique, therefore, is driven by cyclonic circulation around a semi-permanent heat low—the Angola Low—that is typically positioned to the west of Mozambique around the border of Angola and Namibia (Figure 7b), in addition to onshore flow onto southern Mozambique from the subtropical Mascarene High. During an El Niño event, there is a reduction in the strength of trade winds in the tropical Atlantic with a corresponding decrease of evaporative heat flux and delayed SST warming in the region (Enfield & Mayer, 1997; Karnauskas et al., 2008). The resultant Rossby wave train (Figure 7c) leads to an upper-level geopotential height anomaly over southern Africa which, in the case of La Niña (El Niño), leads to a deepening (weakening) of the Angola Low at lower levels (Figure 7d) on average.

The above-described global-scale response leads to regional-scale changes in the lower-level circulation patterns over Mozambique, notably an increase in northwesterly flow over central Mozambique. These

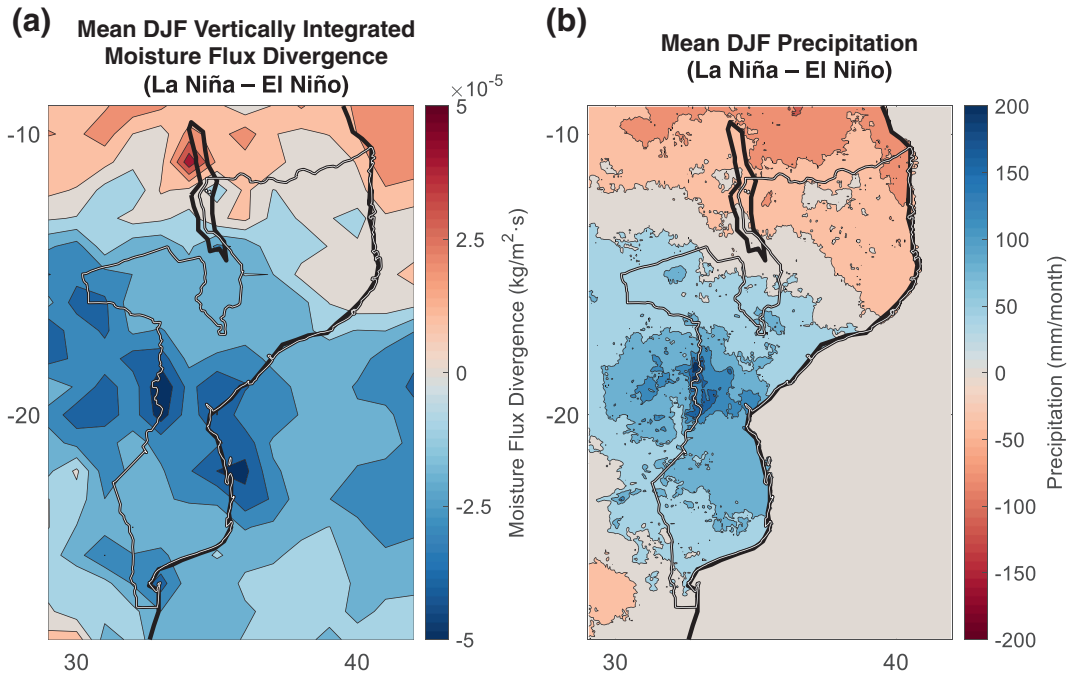

Figure 8. Composite differences in moisture flux divergence and precipitation between La Niña and El Niño in austral summer. (a) Moisture flux divergence in kg/m^2 s (blue-red fill) with contours every 10^{-6} kg/m^2 s. (b) Precipitation in mm/month (red-blue fill) with contours every 50 mm/month.

mean circulation changes caused by the intensification (weakening) of the Angola Low that occurs during La Niña (El Niño) events broadly results in an increase (decrease) in vertically integrated moisture flux convergence and over southern Africa (Figure 7e) and, in particular, over central Mozambique (Figure 8a). This increase in vertically integrated moisture flux convergence directly leads to an increase in precipitation (Figure 8b) and ultimately produces the patterns of malaria and precipitation illustrated in M-EOF1 and P-EOF1 in Figures 4 and 6, respectively.

3.3. Role of Other Modes of Climate Variability

As described in Section 3.1, M-PC2 is highly correlated ($r = -0.80$, $p < 0.001$) with the IOD. However, the canonical influences of the IOD over southern and eastern Africa precipitation do not project onto the precipitation pattern embodied by M-EOF2. A composite of CHIRPS precipitation data on an IOD index reveals a universal increase in precipitation across Mozambique for *positive IOD* (Figure S3). This coincides with neither the pattern (north-south dipole) nor the direction of the primary loading maximum revealed by the secondary EOF pattern in malaria. In addition, P-PC2 over Mozambique from year-to-year is not significantly correlated with the IOD.

Despite the statistically significant correlation between the second EOF of malaria and the IOD, broadening the analysis period using CHIRPS precipitation data reveals the IOD to be an insignificant driver of precipitation in Mozambique over the 1982–2019 time period. Conversely, the SIOD is significantly anticorrelated ($r = -0.35$, $p < 0.05$) with P-PC2 (Figure 6b). Given the relatively recent discovery of the SIOD and relative dearth of literature documenting its regional impacts, we thus explore the physical links between the SIOD and Mozambican precipitation. The field correlation between P-PC2 and global SST anomalies reveals a couplet of anomalously warm and cool SST near the conventional SIOD index boxes (Figure 9a). Though the SIOD index has been conventionally defined (Behera & Yamagata, 2001), there is ongoing debate about the geographic aspect of this metric (Zhang et al., 2019). In an effort to enhance the SIOD index for the present study, we slightly redefine the SIOD index boxes over the regions of highest correlation between SST anomalies and the second principal component of precipitation (Table S1 and Figure 9). The former and modified SIOD indices are significantly correlated ($r = 0.68$, $p < 0.001$), despite the adjustment to align with

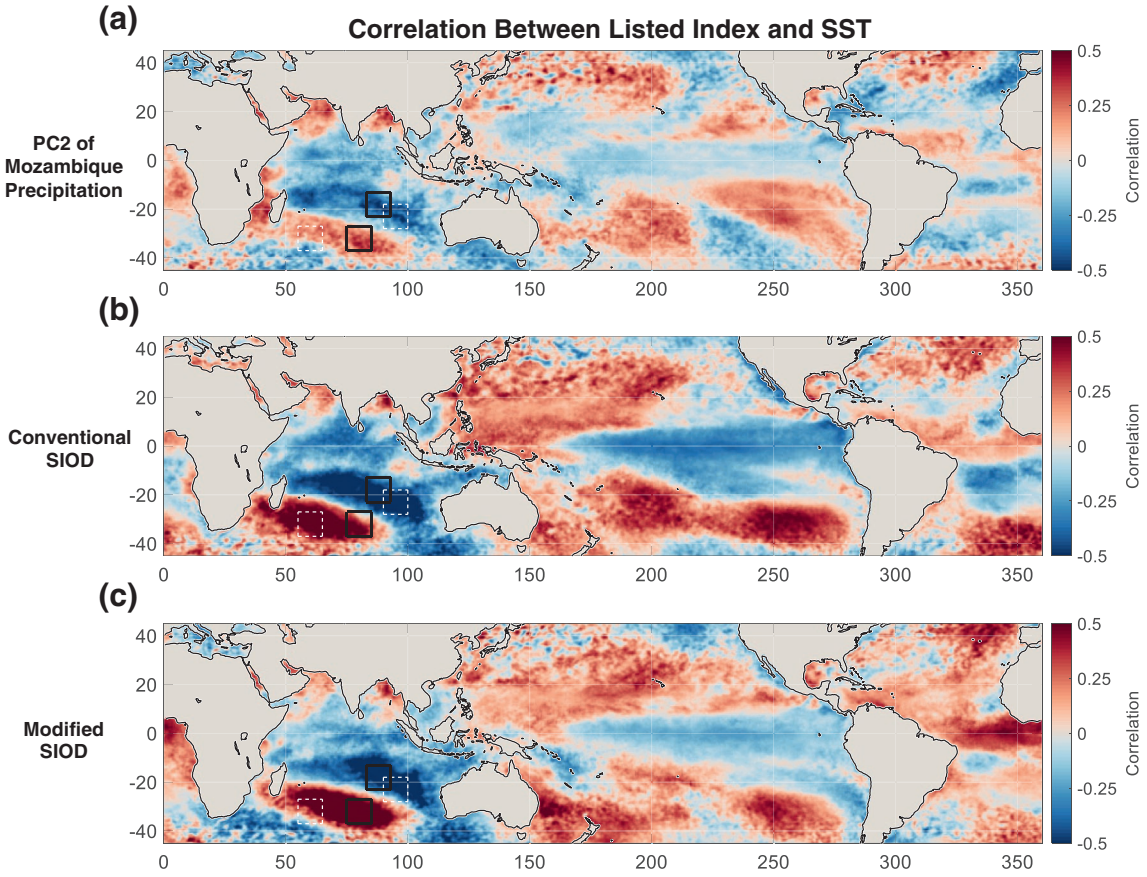

Figure 9. Correlations between global SST fields and various indices. (a) Correlations between austral summer principal component two of long-term precipitation and SSTs (blue-red fill). Conventional and modified SIOD index boxes are outlined in dashed white and solid black, respectively. (b) Same as (a) but for conventional SIOD index and SSTs. (c) Same as (a) but for modified SIOD index and SSTs. SST, sea surface temperatures; SIOD, Subtropical Indian Ocean Dipole.

the relevant SIOD centers of action. In addition to refocusing on the most appropriate areas of the Indian Ocean, evidenced by the increased strength of connection between the SIOD index and P-PC2 (correlation improved from $r = -0.35$ ($p < 0.05$) to $r = -0.46$ ($p < 0.005$)), altering the SIOD index had the additional benefit of reducing the confounding influence of ENSO on the SIOD (strength of correlation decreased from $r = -0.35$ ($p < 0.05$) to $r = -0.19$ [ns]), as shown in Figures 9b and 9c.

There is a strong meridional dipole of spatiotemporal precipitation variability in Mozambique (Figure 10). After calculating the modified SIOD index, field composites of 850 hPa geopotential height and winds (Figure 11a) demonstrate the influence of the SIOD, including mechanistic evidence of the aforementioned meridional dipole of precipitation (Figure 10). As is demonstrated in the composited 850 hPa geopotential height a negative SIOD leads to a weakening of the Mascarene High and the adjacent low-pressure system on average. This produces a low-level circulation pattern where southerly winds enhance onshore flow and lead to moisture flux convergence over the northern part of Mozambique (Figure 11b). This same circulation anomaly leads to moisture flux divergence over the southern part of the country. In contrast, a positive SIOD deepens the Mascarene High and intensifies the adjacent low-pressure system. These changes direct easterly winds toward Madagascar and produce divergent winds and, subsequently, moisture flux divergence over the northern part of the country. This also leads to enhanced moisture advection from the continent and moisture flux convergence over the southern half of Mozambique. These patterns ultimately drive the precipitation response shown in the composite-mean field (Figure 10c), which mirrors P-EOF2 both in austral summer (Figure 10a) and annually (Figure 10b). After ENSO, SIOD is an important secondary factor governing precipitation and, therefore, malaria variability, in Mozambique.

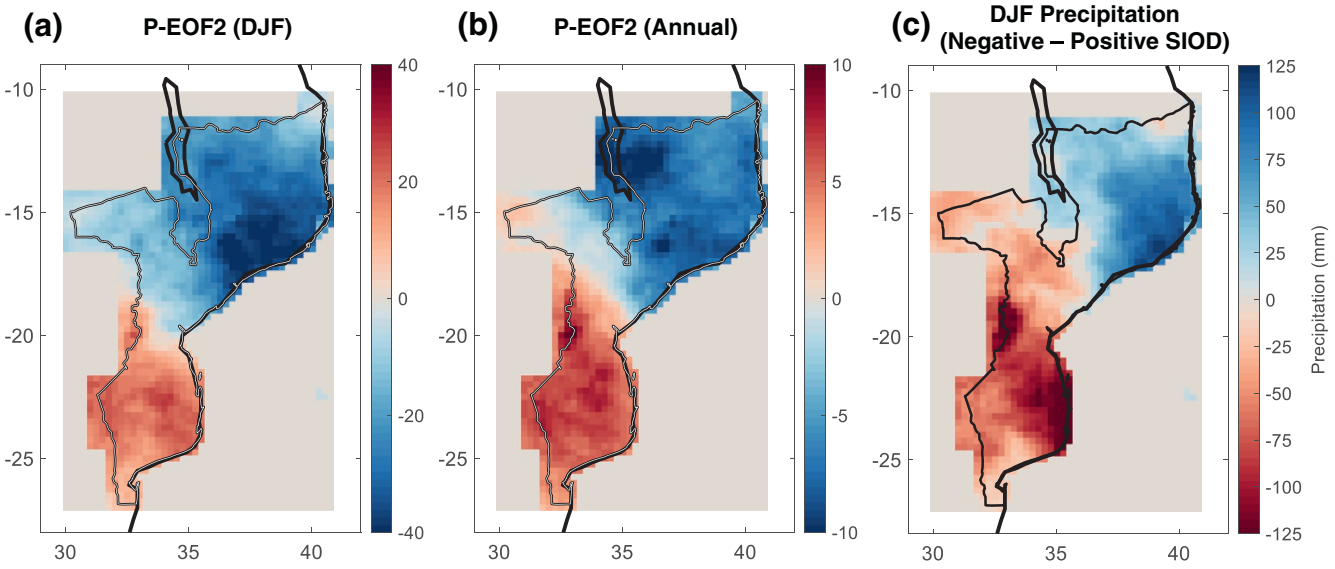

Figure 10. Spatiotemporal patterns in Mozambique precipitation: secondary EOFs and composite of SIOD. (a) Secondary EOF of austral summer precipitation (P-EOF2) in Mozambique (blue-red fill). This mode explains 20.1% of the spatiotemporal variance. (b) Same as (a) but for annual precipitation. This mode explains 17.8% of the spatiotemporal variance. (c) Negative minus positive SIOD composite of austral summer Mozambique precipitation in mm/month (red-blue fill). SIOD, Subtropical Indian Ocean Dipole; EOF, empirical orthogonal function.

4. Summary and Conclusions

This study examined the spatiotemporal variability of malaria and surface climate in Mozambique, based primarily on patterns revealed by two separate EOF analyses—one of malaria incidence for 142 districts in Mozambique, and one of relatively high-resolution precipitation data. Though the primary concern of the analysis is the interannual variability of malaria in Mozambique, utilizing precipitation data as a climate proxy expanded the time period of record and allowed for a more robust comparison with known modes of climate variability.

The leading mode of interannual variability, first revealed through EOF analyses of both malaria and of precipitation, exhibits a primary center of action in the southern part of Mozambique and explains 64% and 46% of the variability in M-EOF1 and P-EOF1, respectively. This loading pattern was statistically and mechanistically linked to ENSO. Anomalous SSTs in the equatorial Pacific associated with a La Niña event

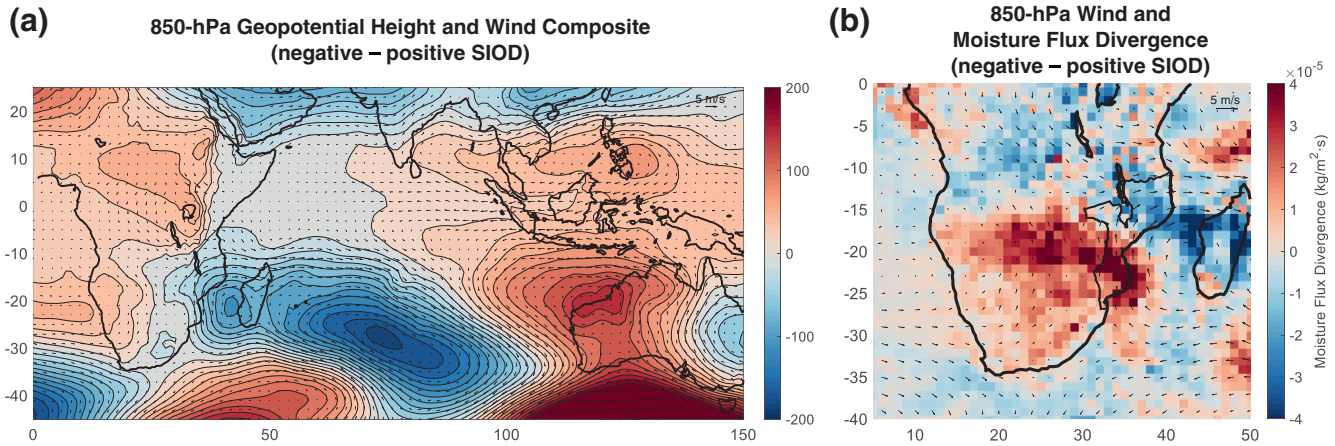

Figure 11. 850 hPa composites over SIOD. (a) Negative minus positive SIOD composite of austral summer 850-hPa geopotential height in m (blue-red fill) and wind vectors. (b) Negative minus positive SIOD composite of vertically integrated moisture flux divergence in kg/m^2 s (blue-red fill) and wind vectors. SIOD, Subtropical Indian Ocean Dipole.

generate atmospheric Rossby and Kelvin waves that produce a cascading global atmospheric response. On average, this forcing leads to a deepening of the Angola Low over southwestern Africa and an intensification of the cyclonic flow in the region. This circulation pattern leads to anomalous advection of moist, tropical air from the Congo Basin toward Mozambique, moisture flux convergence focused over central Mozambique and, ultimately, an increase in precipitation and malaria in the subtropical part of the country. An El Niño event reverses the aforementioned sequence attributable to La Niña events and leads to a decrease in precipitation and malaria in the subtropical part of the country.

Though ENSO is the dominant factor in Mozambique rainfall and the primary driver of malaria in the southern part of the country, we have demonstrated that the SIOD is also an important mode of climate variability over the region. The positive phase of the SIOD generally leads to increased moisture flux convergence and precipitation over the southern part of the country and moisture flux divergence over the northern part of the country. Meanwhile, the negative phase of the SIOD drives onshore flow, increased moisture flux convergence, and enhanced precipitation over the northern part of Mozambique, particularly along the south-facing coast. The SIOD has been demonstrated to be an important, secondary driver of precipitation.

Though the malaria data set used is of high spatial and temporal resolution, the time span of the data is not long enough to confidently establish links with modes of interannual climate variability using solely the malaria record. Given the return period for the relevant climate oscillations investigated—roughly 1–10 years—the length of the time span of the malaria data set provides limited opportunities to perform a robust analysis of climatic influences on malaria incidence. While the strong links between precipitation and malaria do allow for longer-term precipitation data sets to be used as proxies for malaria, this is an assumption with uncertainty. For example, though increased precipitation typically leads to an increase in standing water and mosquito breeding sites, recurring high precipitation events can wash away standing water from previous precipitation events. We are confident in the spatial patterns identified, but the available time period of malaria data is limiting. In addition to data limitations, there is the potential for extrapolation difficulties caused by changes in the strength of modes of climate variability (e.g., Cai et al., 2015, 2019). Notably, there is evidence of a shift in the dominant mode of climate variability in the region from SIOD to ENSO (Richard et al., 2000; Zinke et al., 2004). Finally, we cannot dismiss the possibility that socioeconomic factors (e.g., spatial differences in testing capacity) and intervention coverage and effectiveness may contribute to the spatiotemporal variability of malaria identified in this work, but all analysis indicates these impacts on interannual spatiotemporal variability of malaria are dwarfed by the strength of the previously dissected connections between the spatiotemporal patterns of malaria and modes of climate variability.

The overarching goal of this analysis is to inform a malaria early warning system of benefit to public health officials in Mozambique. By producing what we believe to be a novel application and analysis of an empirical orthogonal function on disease data, we have demonstrated that there may be additional opportunities to inform public health officials by tying broad spatial patterns of malaria rates to quasipredictable modes of climate variability, compared to previously explored models built upon weekly malaria case data and weather predictions. Further research will need to be done to determine if existing intraseasonal and seasonal-to-subseasonal forecasting capabilities allow these connections to be appropriately utilized in a public health setting. In addition, the present malaria data set can be examined on shorter time scales to examine the impacts of temperature and humidity on the spatial patterns observed in the present analysis. Finally, the methodology utilized in the present study may be applied more broadly to other disease data—both to other locations, as well as other species of disease. The use of this methodology in this capacity may reveal both spatial patterns of disease outbreaks and interannual prevalence of disease.

Data Availability Statement

The NOAA Optimal Interpolation version 2 (OIv2) SST and Global Precipitation Climatology Project (GPCP) precipitation data sets are publicly available and can be accessed at https://psl.noaa.gov/data/gridded/data.noaa.oisst.v2.highres.html and https://psl.noaa.gov/data/gridded/data.gpcp.html, respectively. The ECMWF ERA5 reanalysis data are publicly available at https://www.ecmwf.int/en/forecasts/datasets/reanalysis-datasets/era5. Climate Hazards Center CHIRPS data are publicly available at https://www.chc.ucsb.edu/data. All malaria data presented in this study are owned by the Government of Mozambique; they

are available under specific circumstances through a formal request to the Director of the National Malaria Program, Dr Baltazar Candrinho, at candrinhobaltazar@gmail.com.

Acknowledgments
The authors would like to thank the Cooperative Institute for Research in Environmental Sciences for funding of this project through their Innovative Research and Graduate Student Research Award Programs. In addition, the authors would like to thank the Government of Mozambique for access to the malaria data set and acknowledge the NOAA Earth System Research Laboratories for providing OIv2 SST and GPCP precipitation data sets, the ECMWF for providing ERA5 data, and the Climate Hazards Center for providing the CHIRPS dataset. Publication of this article was funded in part by the University of Colorado Boulder Libraries Open Access Fund. Finally, the authors would like to thank Chris Funk, Andrew Hoell, and Andrew Winters for insightful conversations during the formative stages of this project.

References

Adler, R. F., Huffman, G. J., Chang, A., Ferraro, R., Xie, P. P., Janowiak, J., et al. (2003). The version-2 global precipitation climatology project (GPCP) monthly precipitation analysis (1979–present). *Journal of Hydrometeorology*, *4*(6), 1147–1167. https://doi.org/10.1175/1525-7541(2003)004<1147:TVGPCP>2.0.CO;2

Ashok, K., Guan, Z., & Yamagata, T. (2001). Impact of the Indian Ocean dipole on the relationship between the Indian monsoon rainfall and ENSO. *Geophysical Research Letters*, *28*(23), 4499–4502. https://doi.org/10.1029/2001GL013294

Ashok, K., Guan, Z., & Yamagata, T. (2003). Influence of the Indian Ocean Dipole on the Australian winter rainfall. *Geophysical Research Letters*, *30*(15), 1821. https://doi.org/10.1029/2003GL017926

Behera, S. K., Morioka, Y., Ikeda, T., Doi, T., Ratnam, J. V., Nonaka, M., et al. (2018). Malaria incidences in South Africa linked to a climate mode in southwestern Indian Ocean. *Environmental Development*, *27*, 47–57. https://doi.org/10.1016/j.envdev.2018.07.002

Behera, S. K., & Yamagata, T. (2001). Subtropical SST dipole events in the southern Indian Ocean. *Geophysical Research Letters*, *28*(2), 327–330. https://doi.org/10.1029/2000GL011451

Björnsson, H., & Venegas, S. A. (1997). A manual for EOF and SVD analyses of climatic data. *CCGCR Report*, *97*(1), 112–134.

Bouma, M. J., & van der Kaay, H. J. (1996). The EI Niño southern oscillation and the historic malaria epidemics on the Indian subcontinent and Sri Lanka: An early warning system for future epidemics? *Tropical Medicine and International Health*, *1*(1), 86–96. https://doi.org/10.1046/j.1365-3156.1996.d01-7.x

Cai, W., Santoso, A., Wang, G., Yeh, S. W., An, S. I., Cobb, K. M., et al. (2015). ENSO and greenhouse warming. *Nature Climate Change*, *5*(9), 849–859. https://doi.org/10.1038/NCLIMATE2743

Cai, W., Wu, L., Lengaigne, M., Li, T., McGregor, S., Kug, J. S., et al. (2019). Pantropical climate interactions. *Science*, *363*(6430), eaav4236. https://doi.org/10.1126/science.aav4236

Cane, M. A., Eshel, G., & Buckland, R. W. (1994). Forecasting Zimbabwean maize yield using eastern equatorial Pacific sea surface temperature. *Nature*, *370*(6486), 204–205. https://doi.org/10.1038/370204a0

Centers for Disease Control and Prevention. (2018a). Malaria's impact worldwide. Retrieved from https://www.cdc.gov/malaria/malaria_worldwide/impact.html

Centers for Disease Control and Prevention. (2018b). About malaria: Biology. Retrieved from https://www.cdc.gov/malaria/about/biology/index.html

Centers for Disease Control and Prevention. (2018c). President's malaria initiative. Retrieved from https://www.cdc.gov/malaria/malaria_worldwide/cdc_activities/pmi.html

Colborn, K. L., Giorgi, E., Monaghan, A. J., Gudo, E., Candrinho, B., Marrufo, T. J., & Colborn, J. M. (2018). Spatio-temporal modelling of weekly malaria incidence in children under 5 for early epidemic detection in Mozambique. *Scientific Reports*, *8*(1), 1–9. https://doi.org/10.1038/s41598-018-27537-4

Copernicus Climate Change Service (C3S). (2017). ERA5: Fifth generation of ECMWF atmospheric reanalyzes of the global climate. Copernicus climate change Service climate data store (CDS). Retrieved from https://cds.climate.copernicus.eu/cdsapp#!/home

Dee, D. P., Uppala, S. M., Simmons, A. J., Berrisford, P., Poli, P., Kobayashi, S., et al. (2011). The ERA-Interim reanalysis: Configuration and performance of the data assimilation system. *Quarterly Journal of the Royal Meteorological Society*, *137*(656), 553–597. https://doi.org/10.1002/qj.828

Diouf, I., Fonseca, B. R., Caminade, C., Thiaw, W. M., Deme, A., Morse, A. P., et al. (2020). Climate variability and malaria over west Africa. *The American Journal of Tropical Medicine and Hygiene*, *102*(5), 1037–1047. https://doi.org/10.4269/ajtmh.19-0062

Enfield, D. B., & Mayer, D. A. (1997). Tropical Atlantic sea surface temperature variability and its relation to El Niño-southern oscillation. *Journal of Geophysical Research*, *102*(C1), 929–945. https://doi.org/10.1029/96JC03296

Florenchie, P., Lutjeharms, J. R., Reason, C. J. C., Masson, S., & Rouault, M. (2003). The source of Benguela Niños in the South Atlantic Ocean. *Geophysical Research Letters*, *30*(10). https://doi.org/10.1029/2003GL017172

Funk, C. C., Peterson, P. J., Landsfeld, M. F., Pedreros, D. H., Verdin, J. P., Rowland, J. D., et al. (2014). A quasi-global precipitation time series for drought monitoring. *US Geological Survey Data Series*, *832*(4), 1–12. https://doi.org/10.3133/ds832

Funk, C., Peterson, P., Landsfeld, M., Pedreros, D., Verdin, J., Shukla, S., et al. (2015). The climate hazards infrared precipitation with stations—a new environmental record for monitoring extremes. *Scientific Data*, *2*(1), 1–21. https://doi.org/10.1038/sdata.2015.66

Gill, A. E. (1980). Some simple solutions for heat-induced tropical circulation. *Quarterly Journal of the Royal Meteorological Society*, *106*(449), 447–462. https://doi.org/10.1002/qj.49710644905

Gillett, N. P., Kell, T. D., & Jones, P. D. (2006). Regional climate impacts of the southern annular mode. *Geophysical Research Letters*, *33*(23), L23704. https://doi.org/10.1029/2006GL027721

Girond, F., Randrianasolo, L., Randriamampionona, L., Rakotomanana, F., Randrianarivelojosia, M., Ratsitorahina, M., et al. (2017). Analyzing trends and forecasting malaria epidemics in Madagascar using a sentinel surveillance network: A web-based application. *Malaria Journal*, *16*(1), 72. https://doi.org/10.1186/s12936-017-1728-9

Gong, D., & Wang, S. (1999). Definition of Antarctic oscillation index. *Geophysical Research Letters*, *26*(4), 459–462. https://doi.org/10.1029/1999GL900003

Hansingo, K., & Reason, C. J. C. (2009). Modelling the atmospheric response over southern Africa to SST forcing in the southeast tropical Atlantic and southwest subtropical Indian Oceans. *International Journal of Climatology: A Journal of the Royal Meteorological Society*, *29*(7), 1001–1012. https://doi.org/10.1002/joc.1919

Hendon, H. H., Thompson, D. W., & Wheeler, M. C. (2007). Australian rainfall and surface temperature variations associated with the Southern Hemisphere annular mode. *Journal of Climate*, *20*(11), 2452–2467. https://doi.org/10.1175/JCLI4134.1

Hennermann, K., & Berrisford, P. (2017). ERA5 data documentation. Copernicus knowledge base.

Hersbach, H., Bell, B., Berrisford, P., Horányi, A., Sabater, J. M., Nicolas, J., et al. (2019). Global reanalysis: Goodbye ERA-interim, hello ERA5. *ECMWF Newsletter*, *159*, 17–24. https://doi.org/10.21957/vf291hehd7

Hoell, A., & Cheng, L. (2018). Austral summer Southern Africa precipitation extremes forced by the El Niño-Southern oscillation and the subtropical Indian Ocean dipole. *Climate Dynamics*, *50*(9–10), 3219–3236. https://doi.org/10.1007/s00382-017-3801-z

Hoskins, B. J., & Karoly, D. J. (1981). The steady linear response of a spherical atmosphere to thermal and orographic forcing. *Journal of the Atmospheric Sciences*, *38*(6), 1179–1196. https://doi.org/10.1175/1520-0469(1981)038<1179:TSLROA>2.0.CO;2
Ikeda, T., Behera, S. K., Morioka, Y., Minakawa, N., Hashizume, M., Tsuzuki, A., et al. (2017). Seasonally lagged effects of climatic factors on malaria incidence in South Africa. *Scientific Reports*, *7*(1), 1–9. https://doi.org/10.1038/s41598-017-02680-6
Karnauskas, K. B., Busalacchi, A. J., & Murtugudde, R. (2008). Low-frequency variability and remote forcing of gap winds over the east Pacific warm pool. *Journal of Climate*, *21*(19), 4901–4918. https://doi.org/10.1175/2008JCLI1771.1
Kim, Y., Ratnam, J. V., Doi, T., Morioka, Y., Behera, S., Tsuzuki, A., et al. (2019). Malaria predictions based on seasonal climate forecasts in South Africa: A time series distributed lag nonlinear model. *Scientific Reports*, *9*(1), 1–10. https://doi.org/10.1038/s41598-019-53838-3
Kreppel, K., Caminade, C., Govella, N., Morse, A. P., Ferguson, H. M., & Baylis, M. (2019). Impact of ENSO 2016–17 on regional climate and malaria vector dynamics in Tanzania. *Environmental Research Letters*, *14*(7), 075009. https://doi.org/10.1088/1748-9326/ab26c7
Landman, W. A., Sweijd, N., Masedi, N., & Minakawa, N. (2020). The development and prudent application of climate-based forecasts of seasonal malaria in the Limpopo province in South Africa *Environmental Development*, *35*, 100522. https://doi.org/10.1016/j.envdev.2020.100522
Mabaso, M. L. H., & Ndlovu, N. C. (2012). Critical review of research literature on climate-driven malaria epidemics in sub-Saharan Africa. *Public Health*, *126*(11), 909–919. https://doi.org/10.1016/j.puhe.2012.07.005
Marshall, G. J. (2003). Trends in the southern annular mode from observations and reanalyzes. *Journal of Climate*, *16*(24), 4134–4143. https://doi.org/10.1175/1520-0442(2003)016<4134:TITSAM>2.0.CO;2
Merkord, C. L., Liu, Y., Mihretie, A., Gebrehiwot, T., Awoke, W., Bayabil, E., et al. (2017). Integrating malaria surveillance with climate data for outbreak detection and forecasting: the EPIDEMIA system. *Malaria Journal*, *16*(1), 89. https://doi.org/10.1186/s12936-017-1735-x
Midekisa, A., Senay, G., Henebry, G. M., Semuniguse, P., & Wimberly, M. C. (2012). Remote sensing-based time series models for malaria early warning in the highlands of Ethiopia. *Malaria Journal*, *11*(1), 165. https://doi.org/10.1186/1475-2875-11-165
Morioka, Y., Engelbrecht, F., & Behera, S. K. (2015). Potential sources of decadal climate variability over southern Africa. *Journal of Climate*, *28*(22), 8695–8709. https://doi.org/10.1175/JCLI-D-15-0201.1
Rasmusson, E. M., & Carpenter, T. H. (1983). The relationship between eastern equatorial Pacific sea surface temperatures and rainfall over India and Sri Lanka. *Monthly Weather Review*, *111*(3), 517–528. https://doi.org/10.1175/1520-0493(1983)111<0517:TRBEEP>2.0.CO;2
Reason, C. J. C. (2001). Subtropical Indian Ocean SST dipole events and southern African rainfall. *Geophysical Research Letters*, *28*(11), 2225–2227. https://doi.org/10.1029/2000GL011451
Reason, C. J. C., Landman, W., & Tennant, W. (2006). Seasonal to decadal prediction of southern African climate and its links with variability of the Atlantic Ocean. *Bulletin of the American Meteorological Society*, *87*(7), 941–956. https://doi.org/10.1175/BAMS-87-7-941
Reason, C. J. C., & Rouault, M. (2005). Links between the Antarctic Oscillation and winter rainfall over western South Africa. *Geophysical Research Letters*, *32*(7), L07705. https://doi.org/10.1029/2005GL022419
Reason, C. J., & Smart, S. (2015). Tropical south east Atlantic warm events and associated rainfall anomalies over southern Africa. *Frontiers in Environmental Science*, *3*, 24. https://doi.org/10.3389/fenvs.2015.00024
Reynolds, R. W., Rayner, N. A., Smith, T. M., Stokes, D. C., & Wang, W. (2002). An improved in situ and satellite SST analysis for climate. *Journal of Climate*, *15*(13), 1609–1625. https://doi.org/10.1175/1520-0442(2002)015<1609:AIISAS>2.0.CO;2
Reynolds, R. W., Smith, T. M., Liu, C., Chelton, D. B., Casey, K. S., & Schlax, M. G. (2007). Daily high-resolution-blended analyses for sea surface temperature. *Journal of Climate*, *20*(22), 5473–5496. https://doi.org/10.1175/2007JCLI1824.1
Richard, Y., Trzaska, S., Roucou, P., & Rouault, M. (2000). Modification of the southern African rainfall variability/ENSO relationship since the late 1960s. *Climate Dynamics*, *16*(12), 883–895. https://doi.org/10.1007/s003820000086
Ropelewski, C. F., & Halpert, M. S. (1987). Global and regional scale precipitation patterns associated with the El Niño/Southern Oscillation. *Monthly Weather Review*, *115*(8), 1606–1626. https://doi.org/10.1175/1520-0493(1987)115<1606:GARSPP>2.0.CO;2
Rouault, M., Florenchie, P., Fauchereau, N., & Reason, C. J. (2003). South East tropical Atlantic warm events and southern African rainfall. *Geophysical Research Letters*, *30*(5), 8009. https://doi.org/10.1029/2002GL014840
Saji, N. H., Goswami, B. N., Vinayachandran, P. N., & Yamagata, T. (1999). A dipole mode in the tropical Indian Ocean. *Nature*, *401*(6751), 360–363. https://doi.org/10.1038/43854
Saji, N. H., & Yamagata, T. (2003). Possible impacts of Indian Ocean dipole mode events on global climate. *Climate Research*, *25*(2), 151–169. https://doi.org/10.3354/cr025151
Shannon, L. V., Boyd, A. J., Brundrit, G. B., & Taunton-Clark, J. (1986). On the existence of an El Niño-type phenomenon in the Benguela system. *Journal of Marine Research*, *44*(3), 495–520. https://doi.org/10.1357/002224086788403105
Smith, J., Tahani, L., Bobogare, A., Bugoro, H., Otto, F., Fafale, G., et al. (2017a). Malaria early warning tool: Linking inter-annual climate and malaria variability in northern Guadalcanal, Solomon Islands. *Malaria Journal*, *16*(1), 472. https://doi.org/10.1186/s12936-017-2120-5
Smith, K. R., Woodward, A., Campbell-Lendrum, D., Chadee, D., Honda, Y., Liu, Q., et al. (2017b). Human health: Impacts, adaptation and co-benefits. In *Climate change 2014: Impacts, adaptation, and vulnerability. Part A: Global and sectoral aspects. Contribution of working group II to the fifth assessment report of the intergovernmental panel on climate change* (pp. 709–754). Cambridge: Cambridge University Press.
Teklehaimanot, H. D., Lipsitch, M., Teklehaimanot, A., & Schwartz, J. (2004). Weather-based prediction of Plasmodium falciparum malaria in epidemic-prone regions of Ethiopia I. Patterns of lagged weather effects reflect biological mechanisms. *Malaria Journal*, *3*(1), 41. https://doi.org/10.1186/1475-2875-3-41
Thomson, M. C., Doblas-Reyes, F. J., Mason, S. J., Hagedorn, R., Connor, S. J., Phindela, T., et al. (2006). Malaria early warnings based on seasonal climate forecasts from multi-model ensembles. *Nature*, *439*(7076), 576–579. https://doi.org/10.1038/nature04503
Thomson, M. C., Muñoz, Á. G., Cousin, R., & Shumake-Guillemot, J. (2018). Climate drivers of vector-borne diseases in Africa and their relevance to control programmes. *Infectious diseases of poverty*, *7*(1), 81. https://doi.org/10.1186/s40249-018-0460-1
Watts, N., Amann, M., Arnell, N., Karlsson, S. A., Belesova, K., Boykoff, M., et al. (2019). The 2019 report of the lancet countdown on health and climate change: Ensuring that the health of a child born today is not defined by a changing climate. *The Lancet*, *394*(10211), 1836–1878. https://doi.org/10.1016/S0140-6736(19)32596-6
Webster, P. J., Moore, A. M., Loschnigg, J. P., & Leben, R. R. (1999). Coupled ocean–atmosphere dynamics in the Indian Ocean during 1997–98. *Nature*, *401*(6751), 356–360. https://doi.org/10.1038/43848
World Health Organization (2001). *Roll back malaria. Malaria early warning system. A framework for field research in Africa: Concepts, indicators and partners*. Geneva: World Health Organization.
World Health Organization (2018a). *Global health estimates 2016: Disease burden by cause, age, sex, by country and by region, 2000–2016*. Geneva: World Health Organization.

World Health Organization (2018b). *Mozambique country profile*. World Health Organization. Retrieved from https://www.who.int/malaria/publications/country-profiles/profile_moz_en.pdf?ua=1

World Health Organization (2020). *Malaria fact sheet*. World Health Organization. Retrieved from https://www.who.int/news-room/fact-sheets/detail/malaria

Xiang, J., Hansen, A., Liu, Q., Tong, M. X., Liu, X., Sun, Y., et al. (2018). Association between malaria incidence and meteorological factors: A multi-location study in China, 2005–2012. *Epidemiology and Infection*, *146*(1), 89–99. https://doi.org/10.1017/S0950268817002254

Zhang, L., Han, W., Li, Y., & Lovenduski, N. S. (2019). Variability of sea level and upper-ocean heat content in the Indian Ocean: Effects of subtropical Indian Ocean Dipole and ENSO. *Journal of Climate*, *32*, 7227–7245. https://doi.org/10.1175/JCLI-D-19-0167.1

Zinke, J., Dullo, W. C., Heiss, G. A., & Eisenhauer, A. (2004). ENSO and Indian Ocean subtropical dipole variability is recorded in a coral record off southwest Madagascar for the period 1659 to 1995. *Earth and Planetary Science Letters*, *228*(1–2), 177–194. https://doi.org/10.1016/j.epsl.2004.09.028